Check for updates

AGU ADVANCING EARTH AND SPACE SCIENCE

JGR Atmospheres

RESEARCH ARTICLE
10.1029/2021JD036011

Key Points:

- The unprecedented extreme rainfall episodes in early-mid summer of 2020 manifest as recurring latitudinal shifts around Yangtse river
- The north-south shifts of 2020 Meiyu rainfall show a high correspondence with the recurring Madden-Julian Oscillation (MJO) Phase 1–2 swings
- The MJO modulates the latitudinal shifts of Meiyu rainfall mainly through changing the westward extended ridge line of western North Pacific anticyclone

Correspondence to:
H.-L. Ren,
renhl@cma.gov.cn

Citation:
Wang, Y., Ren, H.-L., Wei, Y., Jin, F.-F., Ren, P., Gao, L., & Wu, J. (2022). MJO Phase swings modulate the recurring latitudinal shifts of the 2020 extreme summer-monsoon rainfall around Yangtse. *Journal of Geophysical Research: Atmospheres*, *127*, e2021JD036011. https://doi.org/10.1029/2021JD036011

Received 9 OCT 2021
Accepted 9 MAR 2022

© 2022. American Geophysical Union. All Rights Reserved.

MJO Phase Swings Modulate the Recurring Latitudinal Shifts of the 2020 Extreme Summer-Monsoon Rainfall Around Yangtse

Yuwen Wang[1], Hong-Li Ren[1], Yuntao Wei[1,2], Fei-Fei Jin[3], Pengfei Ren[4], Li Gao[5], and Jie Wu[6]

[1]State Key Laboratory of Severe Weather, Chinese Academy of Meteorological Sciences, Beijing, China, [2]Department of Atmospheric and Oceanic Sciences and Institute of Atmospheric Sciences, Fudan University, Shanghai, China, [3]Department of Atmospheric Sciences, School of Ocean and Earth Science and Technology, University of Hawaii at Manoa, Honolulu, HI, USA, [4]Guangdong Meteorological Observatory, Guangdong Meteorological Bureau, Guangzhou, China, [5]CMA Earth System Modeling and Prediction Centre (CEMC), National Meteorological Center, and State Key Laboratory of Severe Weather, Beijing, China, [6]CMA Climate Studies Key Laboratory & CMA-NJU Joint Laboratory for Climate Prediction Studies, National Climate Center, China Meteorological Administration, Beijing, China

Abstract Considering the unprecedented extremity of the Meiyu episodes in early summer of 2020, here the authors perform a comprehensive study of the intraseasonal evolution characteristics of the observed rainfall round Yangtse as well as the potential modulating effect of Madden-Julian Oscillation (MJO). Results suggest that the Meiyu rainfall manifests as recurring latitudinal shifts around Yangtse during June–July of 2020, corresponding well to the continued swings of MJO circulation and convection between Phase 1 and Phase 2. The MJO affects the meridional migration of the 2020 Meiyu rainfall mainly through regulating the westward extended ridge line and southwesterly of the anomalous anticyclone over the western North Pacific (WNP). Specifically, the northeastward propagation of boreal summer MJO from Phase 1 to 2 shifts the ridge line of the anomalous WNP anticyclone northeastward. Consequently, the associated southwesterly anomaly over the southeastern China penetrates to the north of Yangtse and enhances the lower-tropospheric moisture flux convergence, supporting heavy precipitation there. However, when the MJO swings back to Phase 1, the anomalous southwesterly and moisture flux convergence retreat southward, so does the Meiyu rain band. The present results advanced our understanding of the interactions between the latitudinal shifts of extreme Meiyu rainfall episodes and MJO Phase swings.

1. Introduction

As a high-impact weather phenomenon in the global atmosphere, the persistent extreme rainfall (PER) event usually causes severe meteorological disasters, such as urban flooding that damages agricultural production and threatens human being lives (e.g., Chen & Zhai, 2013; Huang et al., 1998; Lyu et al., 2016). The PER of the East Asia is also called Meiyu (in Chinese). The Meiyu rainfall system is generally caused by a planetary-scale Meiyu front—a strong gradient zone of equivalent potential temperature located on the north side of the East Asia summer monsoon. The Meiyu rainfall over the East Asia features multiscale variabilities and is closely related to the atmospheric 10–20-day quasi-biweekly and 30–60-day intraseasonal oscillations (see the recent review by Ding et al. (2020) and references therein). Deeply understanding the variation of the characteristics of PER or Meiyu, such as its intensity, duration, and also spatiotemporal evolution (e.g., Ren & Ren, 2017; Tang et al., 2006; Wang et al., 2014; Wu et al., 2016), under the modulation of large-scale environment conditions (e.g., Chen & Zhai, 2014; Luo & Zhang, 2015; Shang et al., 2019; Wang et al., 2020; Xie et al., 2009) is a prerequisite to identify the window of opportunity for the skillful prediction of extreme rainfall on the time scales of subseasonal to seasonal (S2S) and beyond (Mariotti et al., 2020).

An unprecedented PER event occurred during the boreal summer of 2020 in the southeastern China and caused a huge economic loss of up to 82 billion (e.g., Hua, 2020; Liu et al., 2020; Zhou et al., 2021). Seen from Figure 1a, the seasonal-mean rainfall anomalies during June–July (JJ) of 2020 display a unique zonal-band structure with the heavy precipitation (e.g., >5 mm day^{-1}) aggregating around along the Yangtse river, which is a typical feature of Meiyu that occurs usually over the southeastern China (e.g., Ding & Chan, 2005). To clearly identify the extremity of the 2020 Meiyu rainfall centered around Yangtse river, the probability density functions of daily total precipitation during JJ of each year from 1980 to 2020 are shown in Figure 1b. Before 2020, the rainfall

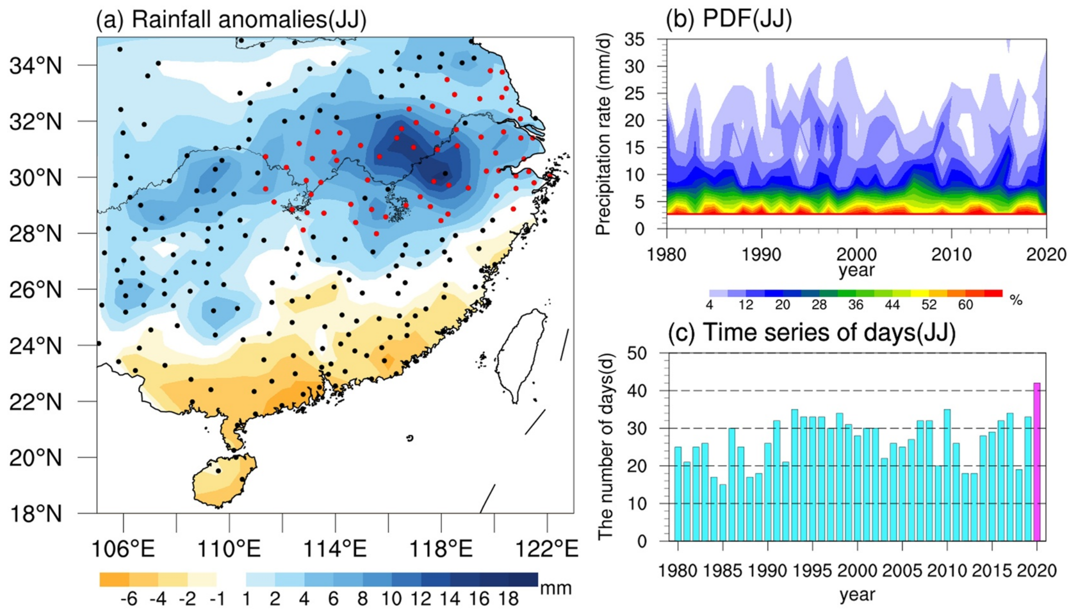

Figure 1. (a) The distribution of rainfall anomalies (mm) in the southeastern China (105°E−123°E, 18°N–35°N) during June–July (JJ) of 2020. Black and red dots represent the geographical distribution of the 262 stations in the southeastern China and the 68 stations in Yangtse river of China, respectively. (b) Temporal evolution of the probability density functions of daily precipitation rate (mm/d) over Yangtse river during JJ in each year of 1980–2020. (c) The time series of the number of days during JJ in each year of 1980–2020 when the precipitation over the southeastern China exceeds its climatology. The magenta bar highlights the year of 2020.

probability during JJ of each year generally decreases exponentially with the increase of rain amount, suggesting the dominant occurrence of light daily-mean rainfall (e.g., <7 mm day^{-1}) in summer. Interestingly, during some years, the small rain rate tends to occur less frequently while the frequency of heavy rainfall is enhanced, such as that during the summers of 1983 and 1998, implying the role of El Niño-Southern Oscillation (ENSO) in interannually regulating the Meiyu over the Yangtse river (e.g., Huang & Wu, 1989). In 2020, the occurrence frequency of weak rain becomes extremely low, and the probability tends to be uniform for the rainfall range of 0–18 mm day^{-1}. Furthermore, the number of days with precipitation exceeding its climatology reaches 42 days, far exceeding those during 1980–2019 (Figure 1c), highlighting the extremely long persistent extreme rainfall episodes in 2020. However, the weak amplitude of ENSO during the summer of 2020 implies that other factors would be at work in affecting this record-breaking PER event.

Among others, the enhanced Meiyu in early–mid summer 2020 was likely associated with the coherent sea surface temperature (SST) warming over the Indian Ocean (IO) which can be traced back to the super Indian Ocean Dipole (IOD) event in the autumn of 2019 (Takaya et al., 2020; Zhou et al., 2021). The mid-latitude teleconnection patterns have been suggested to be important in explaining the long duration (~62 days) of this PER event (Qiao et al., 2021). Liu et al. (2020) noted that the stepwise swing of Meiyu front during JJ 2020 followed the phase transition of North Atlantic Oscillation (NAO). Specifically, in the warm-front stage during June 12–25 with a positive NAO phase, the enhanced rainfall was located to the north of Yangtse river and sustained by the interaction between the South Asian High (SAH) and the western Pacific subtropical high. In contrast, the rain band retreated to the south of Yangtse river in the cold-front stage with a negative NAO phase from 30 June to 13 July due to the coupling between the SAH and mid-latitude Mongolian Cyclone. Motivated by Liu et al. (2020), here we are going to focus on an exploration about the unique north-south migration of Meiyu rainfall with time during JJ 2020. Interestingly, we have found that the PER event undergoes recurring latitudinal shifts in the maximal precipitation center during JJ 2020, which cannot be well explained by the only one-time phase transition of NAO. Instead, we pay our attention to the potential role of Madden-Julian Oscillation (MJO; Madden & Julian, 1971, 1972).

The MJO is the dominant mode of tropical 20–100-day intraseasonal variability (Zhang, 2005), but can cast significant impacts on the weather and climate worldwide (Liebmann et al., 1994; Zhang, 2013). The MJO during boreal summer features a northeastward propagation over the Indian and Asian summer monsoon regions (Kikuchi, 2020). In some specific Phases of MJO, the large-scale circulation anomalies coupled with deep convection may significantly influence the occurrence frequency of extreme rainfall over the southeastern China (Hsu et al., 2016; Ren et al., 2018). For example, Ren and Ren (2017) concluded that the frequency of extreme rainfall frequency during November–March in the southern China was enhanced in MJO Phases 2–3 with a high likelihood due to the strengthened moisture convergence and vertical moisture advection. Roxy et al. (2019) pointed out that the Southeast Asian heavy rainfall in 2011 was consistent with the long-standing MJO activity in Phases 5–7. The possible role of MJO in sustaining the 2020 PER event was firstly suggested by Zhang et al. (2021). They argued that it was not the pronounced IO warming but the exceptionally persistent MJO activity in the IO that played a major role in explaining the extreme Meiyu event of 2020. However, due to compositing the entire Meiyu season, they filtered out the intraseasonal spatiotemporal evolution characteristics of large-scale convection and circulation, and also consequently, the recurring latitudinal shifts observed in the 2020 Meiyu rainfall.

Based on the above reviews, we put forward here the main scientific questions to be addressed in this study: (a) what are the intraseasonal characteristics of the PER event in its spatial and temporal evolutions during the early–mid summer of 2020? (b) Whether and how the intraseasonal conditions associated with the MJOs play a role in shaping the unique intraseasonal variations of the 2020 Meiyu event? Since obtaining accurate information of precipitation location in more than two weeks advance is so important for the end users of S2S predictions, the answers to these questions will likely provide practical implications for the decision making of meteorological disasters on the intraseasonal time scale. The rest of the paper is structured as follows. Section 2 introduces the data and methods. Section 3 documents the evolution characteristics of the extreme Meiyu during JJ 2020 and its relationship with the MJO. Summary and discussions are given in Section 4.

2. Data and Methods

2.1. Data and Their Pre-Processing

The daily gridded datasets used in this study are as follows: the interpolated outgoing longwave radiation (OLR) from the National Oceanic and Atmospheric Administration (NOAA) with a horizontal resolution of 2.5° × 2.5° from 1 January 1980–31 December 2020 (Liebmann & Smith, 1996); the National Center for Environmental Prediction/National Center for Atmospheric Research (NCEP/NCAR) Reanalysis data (Kalnay et al., 1996), including horizontal winds (u and v) and specific humidity (q) covering the same period as NOAA OLR from surface to 300 hPa. The daily 1/4° SST products of Optimal Interpolated Sea Surface Temperature version 2 (OISSTv2) from the NOAA (Huang et al., 2021; Reynolds et al., 2007). The basic characteristics of MJO, such as its phase, propagation, and amplitude, are described using the daily real-time multivariable MJO (RMM) index (Wheeler & Hendon, 2004; hereafter WH04) provided by the Australian Bureau of Meteorology (http://www.bom.gov.au/climate/mjo/). Details of the RMM index method are given in the following Section 2.2.

To analyze the intraseasonal evolution characteristic of the 2020 extreme Meiyu, we downloaded daily precipitation data set of the Chinese surface climate data (V3.0) from the National Meteorological Information Center of China Meteorological Administration (CMA). CMA collects eight meteorological variables including precipitation from 699 Chinese meteorological stations since 1951. Many researchers have used this precipitation product to investigate the intraseasonal and interannual variations of convective activity over the East Asia (e.g., Ji et al., 2020; Ma et al., 2020). Here, we chose 262 stations in the southeastern China (105°E−123°E, 18°N–35°N; see the black dots in Figure 1a) where Meiyu sometimes occurs, and is especially frequent over the Yangtse river region. We selected 68 stations to represent the Yangtse river basin based on the document of "*Meiyu monitoring indices*" published by the Standardization Administration of China (http://www.cmastd.cn/standardView.jspx?id=2386). We did not consider the stations near 32°N, because missing values existed in those stations and were not helpful for our further analysis. The observed station precipitation during 1980–2020 has been bilinearly interpolated into the horizontal resolution of 2.5° × 2.5° before any manipulation.

The daily anomalies of each variable during 1980–2020 were acquired by removing its climatological annual cycle (mean plus the first three harmonics). A 20–100-day bandpass filtering using the 201-point Lanczos filter

(Duchon, 1979) was performed on the daily anomalies to obtain the intraseasonal-scale signals. The space-time filtering technique developed by Wheeler and Kiladis (1999) was also used in this study. For example, the large-scale envelope of MJO convection can be extracted from the daily OLR anomalies by retaining the Fourier components with zonal wavenumbers from 1 to 8 and frequencies from 1/100 to 1/20 cycle per day (CPD). For the equatorial Rossby (ER) wave, the retained ranges of zonal wavenumbers and frequencies are, respectively, -10 to -1 and 1/100 to 1/10 CPD.

2.2. Methods

2.2.1. The RMM Index Method

With the aim of forecasting and monitoring the status of MJO in a real-time manner, WH04 developed the RMM index, which was calculated by projecting the normalized daily unfiltered anomalies onto the first two multivariate empirical orthogonal function (EOF) patterns (i.e., EOF1 and EOF2) of meridionally (15°S–15°N) averaged OLR and 850- (U850) and 200-hPa (U200) zonal wind anomalies. The unfiltered anomaly was derived as the departure of raw data from the annual cycle plus the mean of the previous 120 days. The MJO status can be monitored with a high fidelity through the phase diagram of the two components of RMM index, that is, RMM1 and RMM2. According to the eastward propagation of MJO along the equator, the MJO life cycle can be divided into eight phases based on the RMM index, which correspond to different locations of tropical convective centers of MJO, including the IO (Phases 2–3), Maritime Continent (MC; Phases 4–5), western Pacific (Phases 6–7), and Western Hemisphere/Africa (Phases 8 and 1). Significant MJO events are identified when the RMM amplitude $\sqrt{\mathrm{RMM1}^2+\mathrm{RMM2}^2}$ is greater than one and the trajectory of the phase points shows an anticlockwise rotation for several days. Eastward or westward propagating signals embedded in the unfiltered fields can be further isolated through the reconstruction of convection and circulation (i.e., RMM1×EOF1 + RMM2×EOF2).

The RMM index has been widely used in scientific researches and operational predictions (e.g., Mariotti et al., 2020), though previous studies have revealed its shortcomings in several aspects (e.g., Li et al., 2015; Straub, 2013). The practical advantages of calculating the RMM index through the unfiltering method may in turn changllenge its effectiveness in characterizing the "pure" MJO behaviors. For example, some studies indicated that the high-frequency (<20 days) synoptic-scale waves may have explained some noisy natures of the total RMM index (e.g., Roundy et al., 2009). Also being noted here is that the low-frequency background state may also project onto the spatical pattern of RMM EOF modes, considering that the "120-day running mean" may imperfectly remove the influences of such as the interannual variabilities. During the Meiyu season of 2020, the pronounced SST warming induced by the IOD has been observed over the IO (Takaya et al., 2020). In this study, we will thus consider the possible influences of the IOD, if any, remaining in the OLR and 850-hPa zonal wind anomalies after a 120-day running mean (hereafter, the remaining IOD) on the RMM index-Meiyu association during JJ 2020.

The steps to derive the remaining IOD are as follows. First, we use daily OISSTv2 products to calculate the daily dipole model index (DMI) during JJ 2020, that is, the SST difference between the western Indian Ocean (50°–70°E,10°S–10°N) and the eastern one (90°–110°E, 10°S–0°). Second, the daily OLR, U850 and U200 are then regressed against the normalized resulting DMI. Third, the regressed patterns and normalized daily DMI (with the most recent 120-day mean removed) are used to reconstruct daily evolution of OLR, U850, and U200. These reconstructed fields are the so-called "remaining IOD". Finally, we implement the RMM calculation procedure (Gottschalck et al., 2010), but replace the "unfiltered anomalies" by the "remaining IOD". The output RMM indices are named "RMM-rIOD".

2.2.2. Application of the RMM Index

Based on the RMM method, the phase-dependent influences of MJO can be isolated through the composite conditionally by different MJO phases. Following WH04, we composite the days when the RMM amplitude is larger than one. During JJ 2020, only two days had RMM amplitude smaller than one, but this did not affect our results with or without considering the two days. For example, during the Meiyu season of JJ 2020, 33 days were identified as the MJO Phase 1, which consists of the time periods of June 1–8, June 20–July 10, and July 18–21.

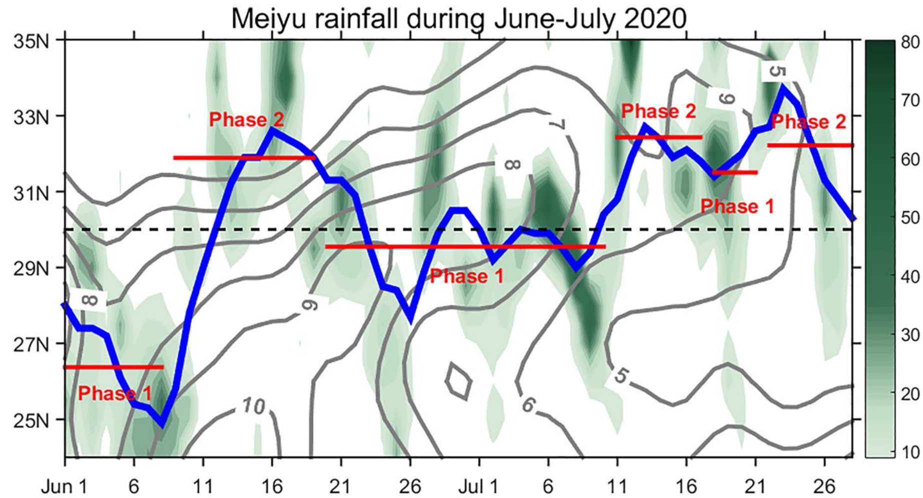

Figure 2. Latitudinal Shifts of the original rainfall (shading; mm) averaged over the longitude band of 105°E−122°E in the southeastern China from June 1 to July 28 of 2020. The gray contours, drawn starting from 5 mm with the contour interval of 1 mm, denote the climatological Meiyu rainfall during June-July of 1980–2019. The blue line indicates the 5-day running mean of the daily occurrence latitude of the maximal rain rate. The red segment lines correspond to the averaged latitude of the daily maximal rain rate for each RMM phase period (i.e., Phases 1 and 2). The horizontal dashed line denotes the approximate latitude location of Yangtse river.

Besides, there are also 23 days corresponding to the MJO Phase 2, which covers June 9–19, July 11, July 14–17, and July 22–28. Therefore, the composite can be made for all the phase-1 (phase-2) days or be made conditionally by different periods of Phase 1 (2). Long-term statistical analysis of 1980–2019 will be also performed to compare the case results of 2020. The significance of the composite is assessed by the two-tailed Student-t test at the 90% confidence level. Besides nonlinear composite analysis, our study also employs linear regression and correlation methods. Specifically, we used the RMM Phase angle (arctan RMM1/RMM2) or RMM amplitude during JJ 2020 as a reference time series to derive the linear dependence of the 2020 PER variation on the MJO. More details in the usage of these analysis methods will be given in the Results section as follows.

3. Results

3.1. Intraseasonal Evolution of the 2020 PER Event: Recurring Latitudinal Shifts Around Yangtse

Before discussing the evolution characteristics of the 2020 PER event, it is necessary to examine the climatological features of the Meiyu season over the southeastern China. In Figure 2, we show the daily precipitation evolution in JJ by contours averaged over the longitude band of 105°–122°E during 1980–2019. As we can see, the climatological Meiyu starts from the south of Yangtse river (around 24°N) during early–mid June. Afterward, it migrates slowly toward the north of Yangtse river. The northward propagation of the Meiyu rainfall may be attributed to the complicated interactions among different climate and weather systems, such as the East-Asian summer monsoon system, MJO, western Pacific subtropical high, and mid-latitude cold vortex (e.g., Ding et al., 2020). However, when we focus on one specific Meiyu episode, the evolution characteristics may be far different from the climatology, because the controlling factors, say those mentioned above, may vary in different years. For example, the eastward propagation of MJO across the MC may be blocked in some years due to the change of mean states (Wei & Ren, 2019; Zhang & Ling, 2017). As a result, the persistent convective activity of MJO over the IO may exert different influences on the extreme rainfall over the southeastern China (e.g., Zhang et al., 2021).

With the above considerations, we further show the time-latitude section of the original rainfall for this extreme Meiyu case of 2020 (see shading in Figure 2). Similar to the climatological characteristics, the total rainfall of JJ 2020 generally manifests as a northward-propagating trend. However, there also exist evident intraseasonal variations when one looks into the daily details during JJ 2020. To clearly show the latitudinal location of the Meiyu

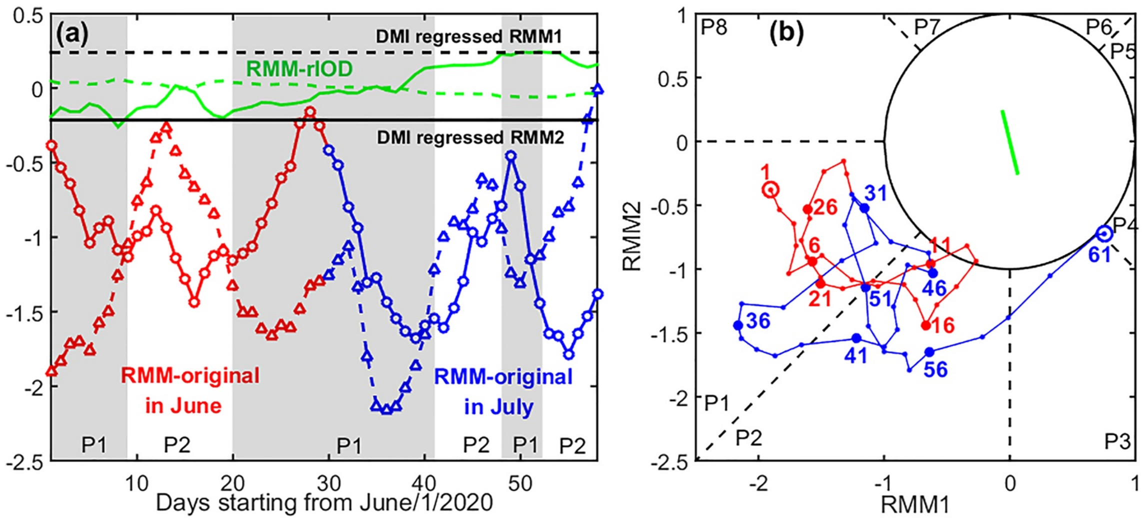

Figure 3. (a) Time evolution of the original RMM indices during June (red) and July (blue) of 2020. Green lines show the RMM indices derived from the remaining IOD (RMM-rIOD; see text for its explanation and calculation). The horizontal black lines denote the regressed RMM indices against the daily dipole mode index (DMI) with the most recent 120-day mean removed. Dashed line denotes RMM1, while solid line is RMM2. Gray (white) background color denotes the stage of RMM Phase 1 (2). (b) Phase diagrams of the original RMM in June (red) and July (blue) 2020 and the RMM-rIOD (green). Note that the axis' range is unsymmetric to clearly show the RMM Phase swing between Phases 1 and 2. The dates (i.e., days since 1 June 2020) are marked by filled circles every five days and dots every one day. The first and the last days are highlighted using larger hollow circles.

rainfall, we further calculate the time evolution of the latitude of daily maximal rain rate (hereafter, Max_Lat) and its 5-day running mean is drawn in Figure 2 as blue line. During early June, the maximal rain rate is located around 26°N, while it jumps to 31°N during middle June. Subsequently, it retreats to the south of 30°N (i.e., the approximate latitude of Yangtse River). Finally, it moves toward the north of Yangtse River after about July 12. Among these recurring latitudinal shifts of the 2020 Meiyu rainfall, the one from mid-June to mid-July has been noted and analyzed by Liu et al. (2020). They suggested that the NAO phase transition may affect the southward shift of Meiyu rainfall. However, the recurring latitudinal shifts of Meiyu rainfall for these PER episodes during the entire Meiyu season of 2020 have not yet been reported. In the following, we try to understand these multiple latitudinal shifts of rain band during JJ 2020 through analyzing some unique characteristics, if any, of MJO during the same period.

3.2. Potential Role of MJO Phase Swings

Before relating the latitudinal shifts of Meiyu rainfall to the MJO impacts, we first diagnose the MJO characteristics themselves during JJ 2020. The original RMM index shows an evident intraseasonal variation with a period of approximately 20 days (Figure 3a). The trajectory of the RMM phase points, which are composed of RMM1 and RMM2, is represented in Figure 3b. It is interesting to note that the RMM index displays recurring swings between Phases 1 and 2 during JJ 2020. More specifically, during June 1–12, the RMM index shows an anticlockwise rotation from MJO Phase 1–2; from June 12–16, a localized growth with standing behavior is observed; while subsequently it turns back to Phase 1 with a clockwise rotation, reflecting the westward-propagating signals during June 16–28. After a long-term persistence (~10 days) in Phase 1 from June 28 to July 7, the RMM index again rotates anticlockwise toward Phase 2. During July 12–17, the amplitude of RMM index decays gradually, while it is still larger than one before swinging back to Phase 1 on July 18. After a short duration (~3 days) in Phase 1 during July 18–21, the RMM index finally rotates anticlockwise toward Phases 2, 3, and beyond, characterizing a typical MJO eastward propagation into the eastern IO and MC. In short, the five-time swings between RMM Phases 1 and 2 give us a new insight into the space-time evolutions of MJO convection and circulation, which is rarely reported in previous studies.

Here, we discuss the possible RMM contribution from the remaining IOD. We first calculate the regressed RMM1 and RMM2 against the daily DMI with the most recent 120-day mean removed. The horizontal black

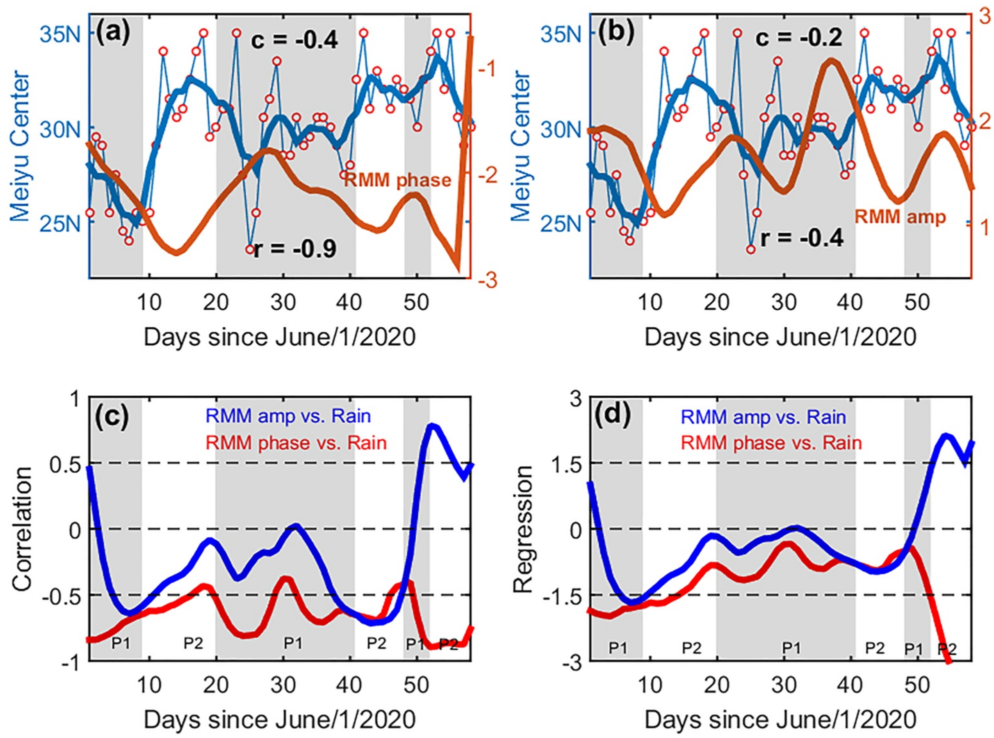

Figure 4. (a) Time evolution of the occurrence latitude of the daily maximal rain rate (Max_Lat, thin blue line with red circle markers) and its 5-day running mean (thick blue) and the RMM Phase angle (brown) during June-July 2020. (b) Same as (a), but for the RMM amplitude. (c) The 20-day running correlation coefficients between the Max_Lat and the RMM amplitude (blue), and also the RMM Phase angle (red). (d) Same as (c), but for the regression coefficients. Gray (white) background color in each subplot denotes stage of RMM Phase 1 (2).

lines in Figure 3a show the regression coefficients, which are much smaller (~±0.25) as compared with the original RMM indices, suggesting the limited role of the remaining IOD in even explaining the RMM amplitude. The RMM-rIOD is rather weak and stays inside the unit circle during JJ 2020 (Figure 3b). Also being noted from Figure 3a is that the first component of RMM-rIOD is nearly zero and the major variation of RMM-rIOD is rooted from its second component (RMM-rIOD2). This suggests that the remaining IOD only contributes to a localized variation of convection and circulation (Figure 3b). Thus, it is the MJO rather than the remaining IOD that contributes to the observed swings of RMM Phases 1 and 2 during JJ 2020. The existence of two MJO events during JJ 2020 is justified in the Appendix.

To detect the potential role of MJO, we give the time evolutions of RMM phases during JJ 2020 and the mean latitudes of rainfall maximum in each MJO phase in Figure 2 (see the red segments). We can see that the recurring latitudinal shifts of maximal rainfall during the 2020 Meiyu season have a high correspondence with the MJO phase swings. More specifically, the northward shifts of Meiyu rainfall generally occur during the stages of MJO Phase 2, while the southward shifts are observed mostly during MJO Phase 1, though some synoptic-scale high-frequency noises are embedded in the day-to-day variation. Therefore, we conjecture that the recurring latitudinal shifts of Meiyu rainfall during early–mid summer of 2020 are probably modulated by the multiple swings of convection and circulation between MJO Phase 1 and Phase 2.

To confirm the role played by the MJO, we first represent the results of linear correlation and regression analyses in Figure 4. Here, both the RMM Phase angle and amplitude are examined. Each variable, including also the Max_Lat, was subjected to a 5-day running mean to highlight the intraseasonal variation. We find from Figure 4a that the RMM Phase angle is generally proportional to the Max_Lat, with a significant negative correlation (c) of −0.4. For example, in several evident southward shifts of Meiyu rainfall, such as those on June 24, July 9, July 20, and July 26, the RMM Phase angle generally displays a local maximum. The Max_Lat also correlates negatively with the RMM amplitude (Figure 4b), but with a weaker magnitude ($c = -0.2$). For the entire Meiyu season

10.1029/2021JD036011

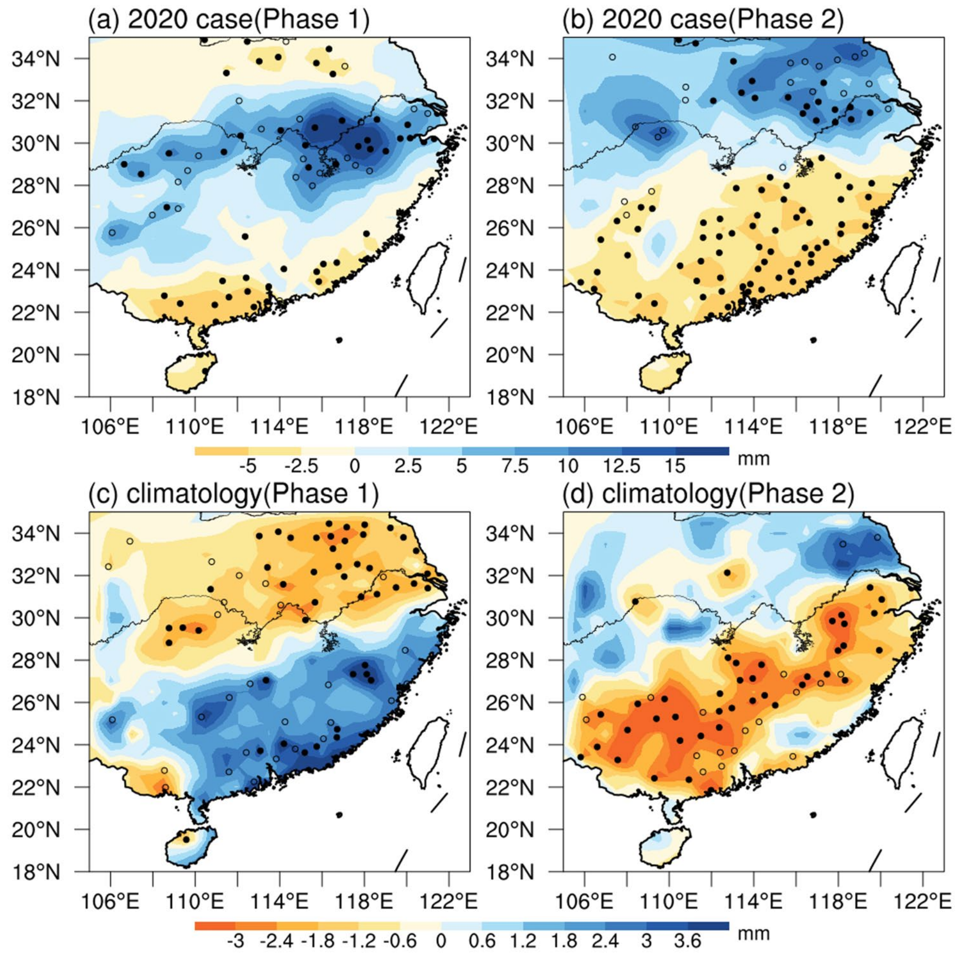

Figure 5. Map of composite rainfall anomalies (mm) in (left) Phase 1 and (right) Phase 2 of active MJO days (i.e., the RMM amplitude > 1.0) over the southeastern China during (a–b) June–July (JJ) of 2020 and (c–d) JJ of 1980–2019. Solid (hollow) circles denote the stations that are statistically significant at the 95% (90%) confidence level. The black curve in each panel shows the basin of the Yangtse river.

during 2020, the regressed (r) Max_Lat against the RMM Phase angle is −0.9, which is stronger than that against the RMM amplitude ($r = -0.4$). The above discussions suggest that the variation of Max_Lat is more related to the change of RMM Phase angle, which can be further proved through a 20-day running window calculation of c (Figure 4c) and r (Figure 4d). The magnitudes of c and r based on the RMM Phase are stronger than those based on the RMM amplitude during most period of JJ 2020.

Also seen from Figure 4, the change of Max_Lat generally follows the transition between RMM Phases 1 and 2. Thus, we secondly composite the anomalous rainfall in RMM Phases 1 and 2 to appreciate the modulation effect of MJO on the Meiyu rainfall of 2020. The results of Phase 1 (33 days) and Phase 2 (23 days) composites during JJ 2020 are showed in Figures 5a and 5b, respectively. In Phase 1, the positive rainfall anomalies are generally located to the south of the Yangtse river, while to the north of 32°N the weak but significant negative rainfall anomalies can be seen. In Phase 2, the enhanced Meiyu rainfall propagates to the north of Yangtse River, while in the south the rainfall is significantly weakened. As a consequence, the northward propagation of Meiyu center 2020 is clearly observed from MJO Phase 1 to Phase 2.

Here is a natural question that to what extent the northward shift of positive rainfall anomalies from MJO Phase 1 to Phase 2 can represent the climatological behaviors of MJO since noises may be involved in the composites of the 2020 case. Thus, we further provide the historical long-term statistical results of the early–mid summer of 1980–2019 (Figures 5c and 5d), in which random noises should be largely smoothed out. Similar to the 2020

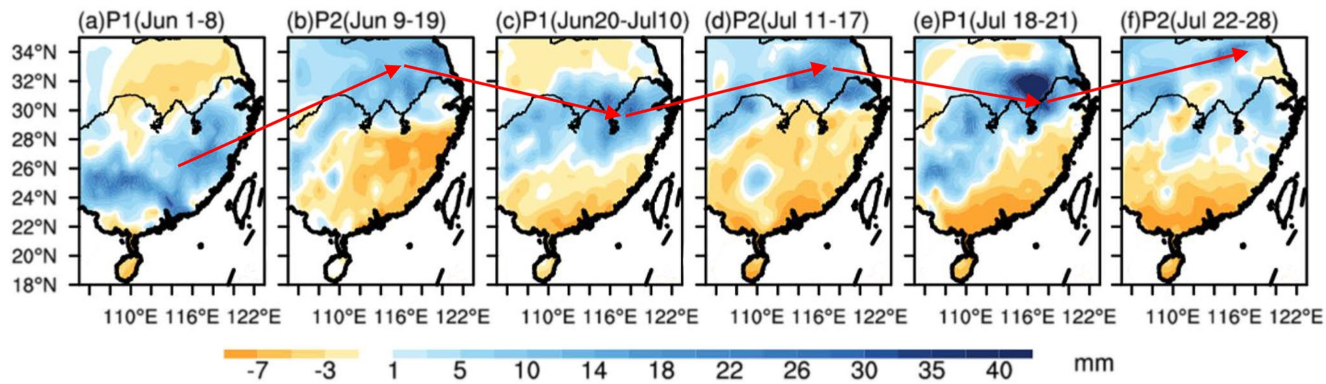

Figure 6. The recurring latitudinal shifts of Meiyu rainfall explained by the multiple MJO Phase swings during June–July 2020. The shading shows the composite total rainfall anomalies (mm) in different RMM Phases 1 and 2. The red arrows direct the meridional propagation trend of enhanced rainfall anomalies between adjacent RMM Phases.

PER case, the enhanced rainfall anomalies in the climatological composite also manifests as the northward propagation from RMM Phase 1 (Figure 5c) to Phase 2 (Figure 5d). In this regard, the latitudinal shifts of anomalous rainfall between RMM Phase 1 and Phase 2 for the 2020 summer is likely a manifestation of the MJO's impacts. Note that the 2020 PER case also differs subtly from the climatology. For example, the composite rainfall anomalies of Phase 1 during 2020 tend to be in quadrature with those of climatology, suggesting that other non-MJO factors, such as the weather and climate systems of mid-high latitudes (e.g., Liu et al., 2020; Qiao et al., 2021), may work energetically during summer of 2020 to compete with the "pure" MJO effect.

The above analysis has confirmed the role of MJO in the 2020 PER case. Next, we explain how the MJO phase swings (Figure 3b) modulate the recurring latitudinal shifts of the 2020 Meiyu rainfall over the Yangtse River (Figure 2). Our strategy is to composite the total rainfall anomalies conditioned by the different stages of MJO Phases 1 and 2. For example, during JJ 2020, a total of three stages of MJO Phase 1 occurred, and thus we make three Phase 1 composites in Figures 6a, 6c, and 6e. We find that the rainfall patterns of Phase 1 in different stages of JJ 2020 are generally similar, though the maximum rainfall center tends to migrate toward the north under the modulation of large-scale northward propagation of boreal-summer MJO. For the three Phase 2 composites (Figures 6b, 6d, and 6f), the anomalous rainfall patterns are also similar but the enhanced Meiyu center shows a systematically shift to the north of Yangtse river, as compared to the Phase 1 composites. Moreover, this northward shift of Meiyu center becomes especially evident between adjacent Phases 1 and 2 of MJO (e.g., Figures 6a and 6b). Thus, the intuitively weak change of MJO from Phase 1 to Phase 2 in JJ 2020 can do shift the Meiyu center northward of Yangtse. The end-to-end arrows in Figure 6 are used to direct the meridional propagation trend of enhanced rainfall anomalies between adjacent MJO Phases. We find that the propagation pattern is very similar to the 5-day running mean Max_Lat shown in Figures 2 and 4. Therefore, the multiple swings of MJO Phases 1–2 play an important role in modulating the recurring latitudinal shifts of the 2020 Meiyu episodes.

3.3. Mechanism of MJO Phase Swings Modulating Latitudinal Shifts of the 2020 PER Event

The mechanisms of MJO Phases 1–2 in affecting the spatiotemporal evolutions of the convective activity over the southeastern China are firstly interpreted from the perspective of long-term statistical analysis. We give the composite OLR and 850-hPa horizontal wind anomalies in Phases 1 and 2 (Figure 7). In Phase 1 (Figure 7a), there is an anomalous anticyclone over the western North Pacific (WNP), characterizing the Rossby wave response to the suppressed MJO convection over tropical western Pacific (Zhang et al., 2009). The anomalous anticyclone center is near 18°N and the low-level southwesterly wind anomalies are dominated on the northwest flank of the anomalous Rossby gyre. Specially, the westward extended ridge line of the WNP anomalous anticyclone is located along ~15°N over the South China Sea, which is essential for the formation of the active convective centers to the south of Yangtse river that coincide with the geographical locations of positive precipitation anomalies (Figure 5c).

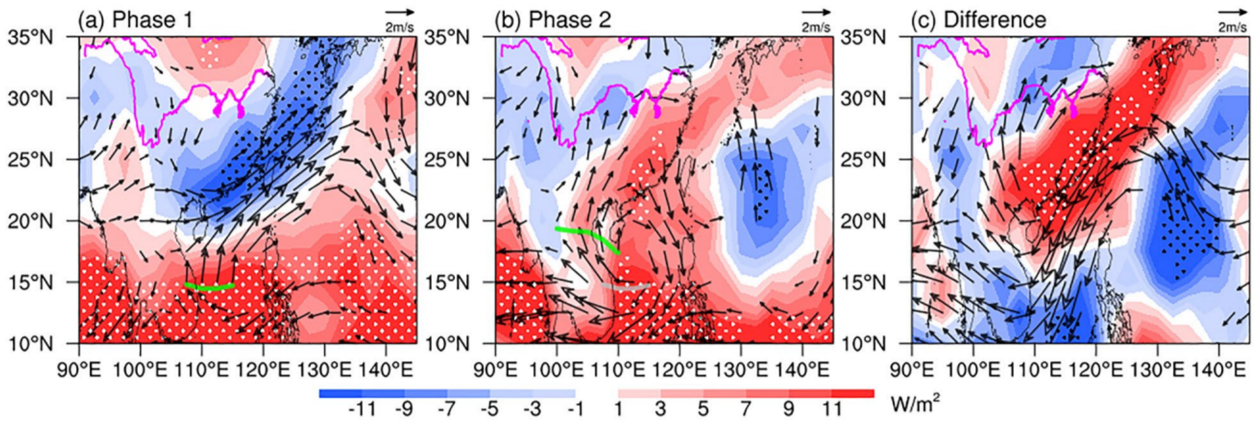

Figure 7. Composite OLR (shading; W/m^2) and 850-hPa horizontal wind anomalies (vectors; m/s) of active MJO days in RMM Phase 1 (a) and Phase 2 (b) during JJ of 1980–2019. (c) The difference of composites between (a) and (b), that is, Phase 2 minus Phase 1. The green curves in panels (a) and (b) denote the westward extended ridge line of the anomalous anticyclone over the western North Pacific. The gray curve in (b) is the ridge line shown in (a) to compare the one in (b). The black (white) dots represent the negative (positive) OLR anomalies significant at the 90% confidence level based on the two-tailed Student *t*'s test. Vectors are shown only for those passing the 90% significance Student *t*'s test. The magenta curves in each panel show the basins of the Yangtse and Yellow rivers.

As compared, in Phase 2 (Figures 7b and 7c), the location of the anomalous anticyclone center is more northern due to the northward propagation of MJO during boreal summer (Lee et al., 2013), particularly accompanied with a northward shifted ridge line (located around 19°N). The southerly component of the anomalous anticyclonic circulation is more evident and converges to the north of Yangtse river, leading to enhanced convection anomalies there. In summary, the MJO in the boreal summer acts to influence the convection and precipitation over the Yangtse river mainly through modulating the latitudinal location and intensity of the anomalous anticyclone over the WNP, of which the westward ridge line and southwesterly wind anomalies might play an essential role.

To demonstrate the critical role of MJO in modulating the recurring latitudinal shifts of the 2020 Meiyu rainfall, we further focus on the intraseasonal evolution of the anomalous WNP anticyclone during JJ 2020. The composites of 850-hPa horizontal winds anomalies conditioned by the MJO Phases are given in Figure 8 that uses a similar presenting style in Figure 6. As one can see, the anomalous anticyclone over the WNP undergoes a vigorous intraseasonal variation, which is clearly reflected by the ridge lines (see red and blue curves in Figure 8) extending westward. With the swings of MJO from Phase 1 (Figures 8a, 8c and 8e) to Phase 2 (Figures 8b, 8d and 8f), the ridge lines also shift northward. As a result, the southwesterly wind anomalies on the northwest flank of the anomalous WNP anticyclone tend to converge to the north of Yangtse river and support the Meiyu rainfall generation there. The above depictions can be observed more clearly by observing the circulation differences between adjacent Phase 2 and Phase 1 (Figures 8g–8i). During the third swing circle of MJO Phases (e.g., Figures 8e and 8f), the strengthened southerly wind anomalies, which converge to the north of Yangtse river, only occur west of 110°E (Figure 8i). Summarized from our discussions above, the MJO acts to influence the recurring north-south shifts of the 2020 Meiyu rainfall mainly through changing the westward extended ridge line of the anomalous WNP anticyclone.

The convergence of 850-hPa wind anomalies may promote the formation of precipitation by accumulating and lifting the *in-situ* humidity. To interpret this mechanism, we diagnose the moisture flux convergence (MFC), which is a good proxy of the deep convection and can be formulated as

$$\mathrm{MFC} = -\nabla \cdot \left(q\vec{V}_h\right) = \underbrace{-\vec{V}_h \cdot \nabla q}_{\textit{Advection term}} \ \underbrace{-q\nabla \cdot \vec{V}_h}_{\textit{Convergence term}}, \tag{1}$$

where $\vec{V}_h = (u, v)$ is the horizontal wind. Equation 1 suggests that MFC can be further decomposed into two components, that is, the moisture advection and convergence terms. We have compared the two terms, while the magnitude of the moisture advection term is small, which is especially true over our target region of Yangtse river and thus is not represented here.

10.1029/2021JD036011

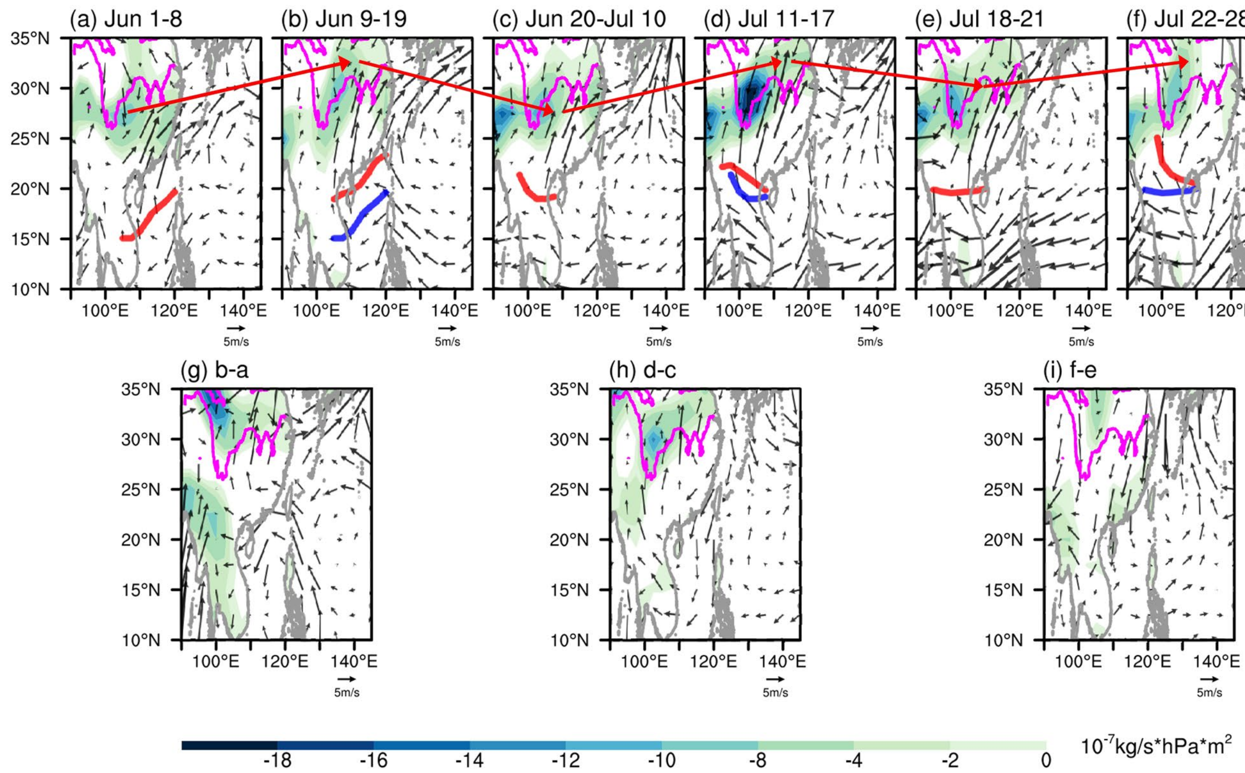

Figure 8. (Upper) Composite horizontal wind (vectors; m/s) and the moisture flux convergence anomalies (shading; 10^{-7} kg s^{-1} hPa^{-1} m^{-2}) at 850 hPa in different stages of RMM Phases 1 (a, c, and e) and 2 (b, d, and f). The red curves indicate the westward extended ridge line of the western North Pacific (WNP) anomalous anticyclone circulation. The blue curves are the copy of the ridge lines in the left adjacent Phase 1 composite. The red arrows direct the meridional propagation trend of anomalous moisture flux convergence between adjacent RMM Phases. (Lower) The differences of composite between adjacent Phase 2 and Phase 1 (g, h, and i). The magenta curves in each panel show the basins of the Yangtse and Yellow rivers.

The shading in Figure 8 shows the composite 850-hPa MFC conditioned by three stages of RMM Phases 1 and 2, along with the differences between adjacent Phase 2 and Phase 1. The convergence center shows similar latitudinal shifts as the 2020 Meiyu rainfall shown in Figure 6, that is, jumping from the south to the north of Yangtse river under the modulation of the northward migration of the ridge line of the anomalous WNP anticyclone when the MJO swings from Phase 1 to Phase 2. A southward propagation of the convergence center is observed, however, when MJO evolves from Phase 2 to Phase 1 (Figures 8g–8i). Figure 9 further presents the latitude-time section of the convergence term of 850-hPa MFC to observe its continuous variation and the correspondence with the evolution of the ridge line of the anomalous WNP anticyclone and the latitude location of Meiyu rainfall averaged in each MJO Phases. Similar to the precipitation evolution (Figure 2), the moisture convergence center shows recurring latitudinal shifts embedded in the large-scale northward propagation, suggesting the close association of the precipitation formation with the lower-tropospheric moisture convergence. Also being noted is the well correspondence between the north-south shifts of the anomalous WNP anticyclone ridge line and those of the Meiyu rainfall, highlighting the modulating effect of the anomalous WNP anticyclone on the intraseasonal shifts of the 2020 PER event.

In summary, our results indicate that the key to affecting the recurring latitudinal shifts of deep convection around Yangtse river during JJ 2020 is the multiple adjustments of MFC (dominated by the moisture convergence term) caused by the variation of anomalous WNP anticyclone with its ridge line latitudinally shifting under the modulation of MJO Phase swings.

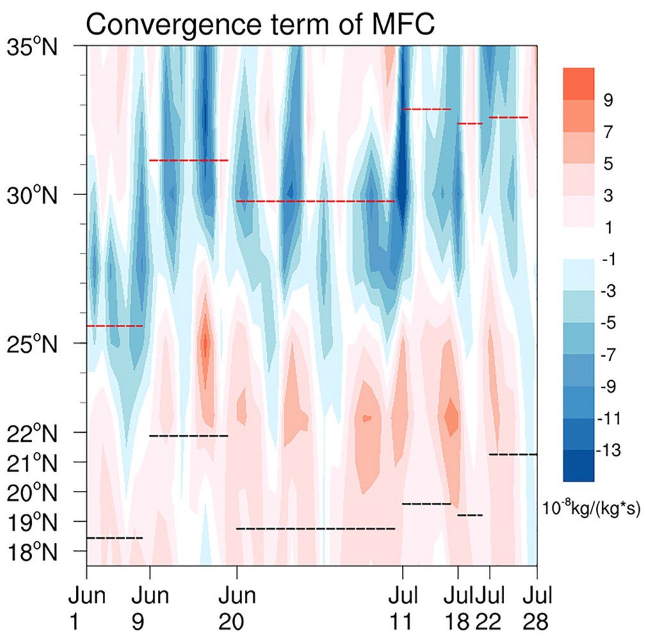

Figure 9. Latitudinal shifts of convergence terms of 850-hPa moisture flux convergence (shading; 10^{-8} kg kg^{-1} s^{-1}) averaged over the longitude band (105°E−122°E) of southeastern China from June 1 to July 28 of 2020. Black and red lines respectively correspond to the mean latitudinal locations of westward extended ridge line for each RMM phase period in Figure 8 and the averaged latitudes in Figure 2.

4. Summary and Discussions

Deeply understanding the modulating factors of extreme rainfall variation is critical for its prediction on the subseasonal time scale. An unprecedented PER event occurred in early–mid summer 2020 over the southeastern China around Yangtse. Despite the extensive documentation of this record-breaking episode, some fundamental scientific questions remain to be addressed. Here, we used observational and reanalysis data to examine the modulating factor of the intraseasonal evolution of the 2020 Meiyu rainfall, with a particular emphasize on the potential role of MJO. Interestingly, we found that (a) the maximal rainfall centers manifested as recurring latitudinal shifts around Yangtse river; (b) the MJO convection and circulation showed several continued swings between MJO Phases 1 and 2 during the same period. We hypothesized that the MJO Phase swings had likely modulated the recurring latitudinal shifts of this 2020 PER event.

To prove our hypothesis, we used different methods, such as composite, reconstruction, linear regression and correlation, to document the correspondence between the MJO Phase swings and the latitudinal shifts of the 2020 Meiyu rainfall. Results suggested that in MJO Phase 1, the anomalous anticyclone over the WNP, with its westward extended ridge line located near the South China Sea and occurring as a Rossby response to the suppressed MJO convection, involved strong southwesterly winds over the southeastern China, which supported deep convection and precipitation to the south of Yangtse river by converging the *in-situ* moist air. When the MJO swung forward to the Phase 2, however, the center and ridge line of the anomalous WNP anticyclone were shifted to the north along the coastal region due to the northeastward propagation of MJO convection and circulation. As a result, the southwesterly wind anomalies on the northwest flank of the anomalous anticyclone penetrated to the north of Yangtse river, leading to the northward shift of enhanced moisture convergence and thus increased precipitation there. These mechanisms worked well and alternatively during JJ of 2020, thus explaining the recurring latitudinal shifts of the 2020 extreme Meiyu event.

Our findings summarized above suggest that we may use the MJO Phase swings to predict the possible location of Meiyu rainfall over the southeast China. Since this study had intended to examine the modulating factors of the multiple latitudinal shifts in the 2020 extreme precipitation, the underlying reasons of the MJO Phase swings are not investigated here. Further works should be conducted to explore the mechanisms of MJO swings between RMM Phases 1 and 2. For example, due to the strong dependence of RMM index on the circulation rather than the convection (Straub, 2013), it is interesting to unravel the relative role of convection and circulation in determining the RMM Phase swings. Some caveats also worth being noted in this study. For example, the positive composite rainfall anomalies of MJO Phase 1 for the 2020 PER case dislocate from that of the climatology, although the Phase 2 composites between the two scenarios are much similar. This reflects that other non-MJO factors during 2020 are so vigorous that the "pure" MJO effect might be distorted. Future study should clarifies the relative role of MJO and non-MJO factors in affecting the 2020 Meiyu rainfall variations.

Appendix A

Existence of MJO During JJ 2020

Whether an MJO event was actually present during JJ 2020, provided that the westward propagation was observed in the trajectory of RMM indices (Figure 3b)? We analyzed the Hovmöller diagrams of the filtered and reconstructed OLR and U850 anomalies in Figure A1. The results suggest that there were actually two intraseasonal deep convection events, whose standing characteristics were more profound than its propagating ones (Figure A1a). Nevertheless, the eastward propagations of large-scale deep convection were still observed over the IO. The first convective episode was fast but it was blocked and decayed quickly when approaching the

10.1029/2021JD036011

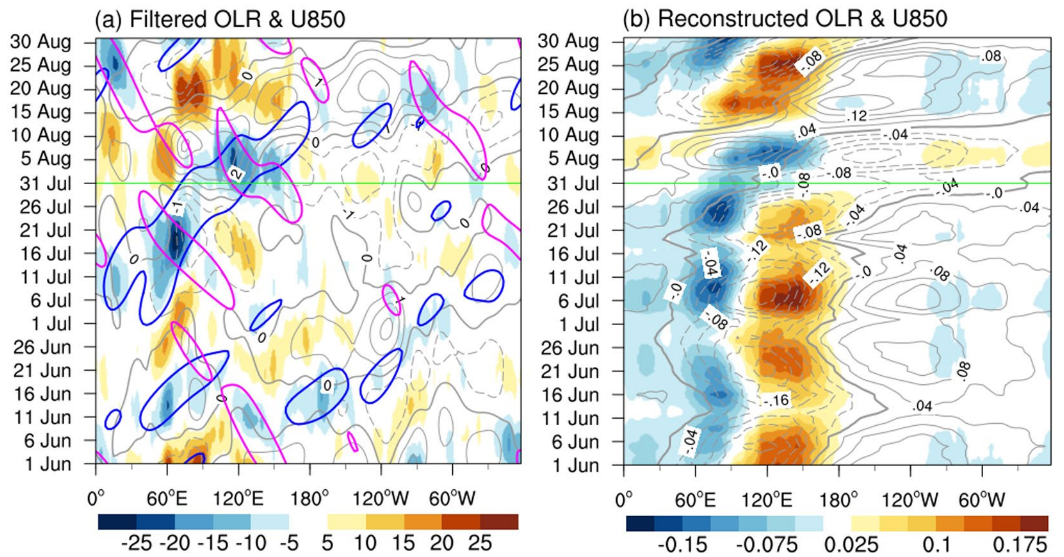

Figure A1. (a) Hovmöller diagram of 20–100-day filtered OLR (shading; W/m^2) and U850 (contour; m/s) anomalies averaged over 15°S–15°N during June-August (JJA) of 2020. The MJO-filtered OLR anomalies smaller than -5 W/m^2 are outlined by thick blue contours. The equatorial Rossby (ER) wave-filtered OLR anomalies smaller than -5 W/m^2 are outlined by thick magenta contours. (b) Hovmöller diagram of the normalized reconstructed 850-hPa (blue contour) and OLR (shading) anomalies during JJA of 2020. Positive (negative) wind anomalies are indicated by solid (dotted) line. The horizontal green line isolates June-July and August of 2020.

western MC. Thus, we might call this intraseasonal convection event the nonpropagating MJO (Kim et al., 2014). In contrast, the second convective episode was slow and also decayed when encountering the MC barrier effect (Zhang & Ling, 2017). However, it tended to jump into the western Pacific during early August 2020. According to Wang et al. (2019), we might call this episode the "jumping" MJO.

The recurring swing of RMM indices implied the occurrence of westward propagation during JJ 2020, which may hinder us to relate the RMM behaviors to the MJO. However, we noted that the most evident westward propagation actually occurred in the second half of June 2020, whereas the other periods of JJ 2020 were dominated by the eastward propagation and standing oscillations (see Figures 3b and A1b). Moreover, the most evident westward propagation started from ~June 15, on which the first MJO deep convection decayed due to the MC barrier effect (Figure 4a). Consequently, the circulation likely did not couple tightly with the MJO deep convection and thus the equatorial westerly wind anomalies, which were the ER wave responses to the deep convection, tended to migrate westward since ~June 15 (Figure A1a). The relaxed coupling of ER wave with the MJO deep convection may be appreciated more clearly from the westward-propagating ER wave-filtered convective envelope from June 17 (see magenta line in Figure A1a). In this regard, the westward propagation activity was intrinsically induced by the decaying deep convection of MJO, because of which the westerly wind's coupling degree relaxed a bit and migrated westward.

In a summary, there actually existed two MJO episodes during JJ 2020, one fast nonpropagating MJO and the other slow jumping MJO. Due to interacations with the MC or other factors, the circulation signals of MJOs showed alternative eastward and westward propagations and also standing oscillations, explaining the observed swings of RMM Phases.

Data Availability Statement

The daily precipitation data set of the Chinese surface climate data (V3.0) is provided by the National Meteorological Information Center of China Meteorological Administration (http://data.cma.cn/). The daily circulation and OLR data are achieved at the NCEP/NCAR, Physical Sciences Laboratory (https://psl.noaa.gov/data/gridded/tables/daily.html). The daily 1/4° SST products of Optimal Interpolated Sea Surface Temperature version 2 (OISSTv2) are from the NOAA (https://www.psl.noaa.gov/data/gridded/data.noaa.oisst.v2.highres.html). The RMM index is obtained from the Australian Bureau of Meteorology (http://www.bom.gov.au/climate/mjo/).

Acknowledgments

The authors thank three anonymous reviewers for their constructive comments that helped improved this article. This work is jointly supported by the China National Science Foundation Projects (42175015, 42175052, 41875138, and 41905067), the National Key Research and Development Program on Monitoring, Early Warning and Prevention of Major Natural Disaster (2021YFA0718000).

References

Chen, Y., & Zhai, P. (2013). Persistent extreme precipitation events in China during 1951–2010. *Climate Research*, *57*, 143–155. https://doi.org/10.3354/cr01171

Chen, Y., & Zhai, P. (2014). Synoptic-scale precursors of the East Asia/Pacifc teleconnection pattern responsible for persistent extreme precipitation in the Yangtze River valley. *Quarterly Journal of the Royal Meteorological Society*, *141*(689), 1389–1403. https://doi.org/10.1002/qj.2448

Ding, Y. H., & Chan, J. C. L. (2005). The East Asian summer monsoon: An overview. *Meteorology and Atmospheric Physics*, *89*(1), 117–142.

Ding, Y. H., Liang, P., Liu, Y., & Zhang, Y. C. (2020). Multiscale variability of Meiyu and its prediction: A new review. *Journal of Geophysical Research: Atmospheres*, *125*, e2019JD031496. https://doi.org/10.1029/2019jd031496

Duchon, C. E. (1979). Lanczos filtering in one and two dimensions. *Journal of Applied Meteorology*, *18*(8), 1016–1022. https://doi.org/10.1175/1520-0450(1979)018<1016:lfioat>2.0.co;2

Gottschalck, J., Wheeler, M., Weickmann, K., Vitart, F., Savage, N., Lin, H., et al. (2010). A framework for assessing operational Madden–Julian oscillation forecasts: A CLIVAR MJO working group project. *Bulletin of the American Meteorological Society*, *91*(9), 1247–1258. https://doi.org/10.1175/2010BAMS2816.1

Hsu, P. C., Lee, J. Y., & Ha, K. J. (2016). Influence of boreal summer intraseasonal oscillation on rainfall extremes in southern China. *International Journal of Climatology*, *36*(3), 1403–1412. https://doi.org/10.1002/joc.4433

Hua, X. (2020). *China raises flood response to second-highest level*. Xinhua News. Retrieved from http://www.xinhuanet.com/english/2020-07/12/c_139207054.htm

Huang, B. Y., Liu, C. Y., Banzon, V., Freeman, E., Graham, G., HanKins, B., et al. (2021). Improvements of the Daily Optimum Interpolation Sea Surface Temperature (DOISST) Version 2.1. *Journal of Climate*, *34*, 2923–2939. https://doi.org/10.1175/JCLI-D-20-0166.1

Huang, R. H., & Wu, Y. F. (1989). The influence of ENSO on the summer climate change in China and its mechanism [J]. *Advances in Atmospheric Sciences*, *6*(1), 21–32. https://doi.org/10.1007/BF02656915

Huang, R. H., Xu, Y., Wang, P., & Zhou, L. (1998). The features of the catastrophic flood over the Changjiang River basin during the summer of 1998 and cause exploration (in Chinese). *Climatic and Environmental Research*, *3*(04), 300–313. https://doi.org/10.3878/j.issn.1006-9585.1998.04.02

Ji, M. Y., Jiang, Y. Y., Han, X. P., Liu, L., Xu, X. L., Qiao, Z., et al. (2020). *Spatiotemporal relationships between air quality and multiple meteorological parameters in 221 Chinese cities* (p. 2020). https://doi.org/10.1155/2020/6829142

Kalnay, E., Kanamitsu, M., Kistler, R., Collins, W., Deaven, D., Gandin, L., et al. (1996). The NCEP/NCAR 40-Year Reanalysis Project. *Bulletin of the American Meteorological Society*, *77*, 437–471. https://doi.org/10.1175/1520-0477(1996)077<0437:tnyrp>2.0.co;2

Kikuchi, K. (2020). Extension of the bimodal intraseasonal oscillation index using JRA-55 reanalysis. *Climate Dynamics*, *54*, 919–933. https://doi.org/10.1007/s00382-019-05037-z

Kim, D., Kug, J.-S., & Sobel, A. H. (2014). Propagating versus nonpropagating Madden–Julian oscillation events. *Journal of Climate*, *27*, 111–125. https://doi.org/10.1175/JCLI-D-13-00084.1

Lee, J. Y., Wang, B., Wheeler, M. C., Fu, X. H., Waliser, D. E., & Kang, I. S. (2013). Real-time multivariate indices for the boreal summer intraseasonal oscillation over the Asian summer monsoon region. *Climate Dynamics*, *40*(1–2), 493509. https://doi.org/10.1007/s00382-012-1544-4

Li, T., Zhao, C., Hsu, P. C., & Nasuno, T. (2015). MJO initiation processes over the tropical Indian Ocean during DYNAMO/CINDY2011. *Journal of Climate*, *28*(6), 2121–2135. https://doi.org/10.1175/jcli-d-14-00328.1

Liebmann, B., Hendon, H. H., & Glik, J. D. (1994). The relationship between tropical cyclones of the western Pacific and Indian oceans and the Madden-Julian Oscillation. *Journal of the Meteorological Society of Japan. Ser. II*, *72*(3), 401–412. https://doi.org/10.2151/jmsj1965.72.3_401

Liebmann, B., & Smith, C. A. (1996). Description of a complete (interpolated) outgoing longwave radiation dataset. *Bulletin of the American Meteorological Society*, *77*(6), 1275–1277. https://doi.org/10.1175/1520-0477(1996)077<1255:EA>2.0.CO;2

Liu, B. Q., Yan, Y. Y., Zhu, C. W., Ma, S. M., & Li, J. Y. (2020). Record-breaking Meiyu rainfall around Yangtze River in 2020 regulated by the subseasonal phase transition of North Atlantic Oscillation. *Geophysical Research Letters*, *47*, e2020GL090342. https://doi.org/10.1029/2020gl090342

Luo, X., & Zhang, Y. C. (2015). The linkage between upper-level jet streams over East Asia and East Asian winter monsoon variability. *Journal of Climate*, *28*(22), 9013–9028. https://doi.org/10.1175/jcli-d-15-0160.1

Lyu, M. Z., Sheng, L. X., Zhang, Z. S., & Zhang, L. (2016). Distribution and accumulation of soil carbon in temperate wetland, northeast China. *Chinese Geographical Science*, *26*(3), 295–303. https://doi.org/10.1007/s11769-016-0809-y

Ma, B., Zhang, B., Jia, L. G., & Huang, H. (2020). Conditional distribution selection for SPEI-daily and its revealed meteorological drought characteristics in China from 1961 to 2017. *Atmospheric Research*, *246*, 105108. https://doi.org/10.1016/j.atmosres.2020.105108

Madden, R. A., & Julian, P. R. (1971). Detection of a 40-50 day oscillation in the zonal wind in the tropical Pacific. *Journal of the Atmospheric Sciences*, *28*(5), 702–708. https://doi.org/10.1175/1520-0469(1971)028<0702:doadoi>2.0.co;2

Madden, R. A., & Julian, P. R. (1972). Description of global-scale circulation cells in the tropics with a 40-50 day period. *Journal of the Atmospheric Sciences*, *29*, 1109–1123. https://doi.org/10.1175/1520-0469(1972)029<1109:dogscc>2.0.co;2

Mariotti, A., Baggett, C., Barnes, E. A., Becker, E., Butler, A., Collins, D. C., et al. (2020). Windows of opportunity for skillful forecasts subseasonal to seasonal and beyond. *Bulletin of the American Meteorological Society*, *101*, E608–E625. https://doi.org/10.1175/bams-d-18-0326.1

Qiao, S., Chen, D., Wang, B., Cheung, H.-N., Liu, F., Cheng, J., et al. (2021). The longest 2020 Meiyu season over the past 60 years: Subseasonal perspective and its predictions. *Geophysical Research Letters*, *48*, e2021GL093596. https://doi.org/10.1029/2021gl093596

Ren, H.-L., & Ren, P. F. (2017). Impact of Madden-Julian Oscillation upon winter extreme rainfall in southern China: Observations and predictability in CFSv2. *Atmosphere*, *8*(10), 192. https://doi.org/10.3390/atmos8100192

Ren, P. F., Ren, H.-L., Fu, J. X., Wu, J., & Du, L. M. (2018). Impact of boreal summer intraseasonal oscillation on rainfall extremes in southeastern China and its predictability in CFSv2. *Journal of Geophysical Research: Atmospheres*, *123*(9), 4423–4442. https://doi.org/10.1029/2017jd028043

Reynolds, R. W., Smith, T. M., Liu, C. Y., Chelton, D. B., Casey, K. S., & Schlax, M. G. (2007). Daily high-resolution-blended analyses for sea surface temperature. *Journal of Climate*, *20*, 5473–5496. https://doi.org/10.1175/2007JCLI1824.1

Roundy, P. E., Schreck, C. J., & Janiga, M. A. (2009). Contributions of convectively coupled equatorial Rossby waves and Kelvin waves to the real-time multivariate MJO indices. *Monthly Weather Review*, *137*(1), 469–478. https://doi.org/10.1175/2008mwr2595.1

Roxy, M. K., Dasgupta, P., McPhaden, M. J., Suematsu, T., Zhang, C., & Kim, D. (2019). Twofold expansion of the Indo-Pacific warm pool warps the MJO life cycle. *Nature*, *575*(7784), 647–651. https://doi.org/10.1038/s41586-019-1764-4

Shang, W., Ren, X. J., Huang, B., Cubasch, U., & Yang, X. Q. (2019). Subseasonal intensity variation of the South Asian high in relationship to diabatic heating: Observation and CMIP5 models. *Climate Dynamics*, *52*, 2413–2430. https://doi.org/10.1007/s00382-018-4266-4

Straub, K. H. (2013). MJO initiation in the real-time multivariate MJO index. *Journal of Climate*, *26*(4), 1130–1151. https://doi.org/10.1175/jcli-d-12-00074.1

Takaya, Y., Ishikawa, I., Kobayashi, C., Endo, H., & Ose, T. (2020). Enhanced Meiyu–Baiu rainfall in early summer 2020: Aftermath of the 2019 super IOD event. *Geophysical Research Letters*, *47*, e2020GL090671. https://doi.org/10.1029/2020gl090671

Tang, Y., Gan, J., Zhao, L., & Gao, K. (2006). On the climatology of persistent heavy rainfall events in China. *Advances in Atmospheric Sciences*, *23*, 678–692. https://doi.org/10.1007/s00376-006-0678-x

Wang, B., Chen, G. S., & Liu, F. (2019). Diversity of the Madden–Julian Oscillation. *Science Advances*, *5*, eaax0220. https://doi.org/10.1126/sciadv.aax0220

Wang, F., Yang, S., Higgins, W., Li, Q. P., & Zuo, Z. Y. (2014). Long-term changes in total and extreme precipitation over China and the United States and their links to oceanic-atmospheric features. *International Journal of Climatology*, *34*(2), 286–302. https://doi.org/10.1002/joc.3685

Wang, L., Yang, Z. N., Gu, X. H., & Li, J. F. (2020). Linkages between tropical cyclones and extreme precipitation over China and the role of ENSO. *International Journal of Disaster Risk Science*, *11*, 538–553. https://doi.org/10.1007/s13753-020-00285-8

Wei, Y., & Ren, H.-L. (2019). Modulation of ENSO on fast and slow MJO modes during boreal winter. *Journal of Climate*, *32*(21), 7483–7506. https://doi.org/10.1175/jcli-d-19-0013.1

Wheeler, M. C., & Hendon, H. H. (2004). An all-season real-time multivariate MJO index: Development of an index for monitoring and prediction. *Monthly Weather Review*, *132*(8), 1917–1932. https://doi.org/10.1175/1520-0493(2004)132<1917:aarmmi>2.0.co;2

Wheeler, M. C., & Kiladis, G. N. (1999). Convectively coupled equatorial waves: Analysis of clouds in the wavenumber-frequency domain. *Journal of the Atmospheric Sciences*, *56*, 374–399. https://doi.org/10.1175/1520-0469(1999)056%3C0374:CCEWAO%3E2.0.CO;2

Wu, Y. J., Wu, S. Y., Wen, J. H., Xu, M., & Tan, J. G. (2016). Changing characteristics of precipitation in China during 1960-2012. *International Journal of Climatology*, *36*(3), 1387–1402. https://doi.org/10.1002/joc.4432

Xie, S. P., Hu, K., Hafner, J., Tokinaga, H., Du, Y., Huang, G., & Sampe, T. (2009). Indian Ocean capacitor effect on Indo–western Pacific climate during the summer following El Niño. *Journal of Climate*, *22*, 730–747. https://doi.org/10.1175/2008jcli2544.1

Zhang, C. (2005). Madden-Julian Oscillation. *Reviews of Geophysics*, *43*(2), RG2003. https://doi.org/10.1029/2004rg000158

Zhang, C. (2013). Madden-Julian Oscillation: Bridging weather and climate. *Bulletin of the American Meteorological Society*, *69*(1), 65–78. https://doi.org/10.1175/bams-d-12-00026.1

Zhang, C., & Ling, J. (2017). Barrier effect of the Indo-Pacific Maritime Continent on the MJO: Perspectives from tracking MJO precipitation. *Journal of Climate*, *30*(9), 3439–3459. https://doi.org/10.1175/jcli-d-16-0614.1

Zhang, L. N., Wang, B. Z., & Zeng, Q. C. (2009). Impact of the Madden-Julian Oscillation on Summer Rainfall in Southeast China. *Journal of Climate*, *22*(2), 201–216. https://doi.org/10.1175/2008JCLI1959.1

Zhang, W. J., Huang, Z. C., Jiang, F., Stuecker, M. F., Chen, G. S., & Jin, F. F. (2021). Exceptionally persistent Madden-Julian Oscillation activity contributes to the extreme 2020 East Asian summer monsoon rainfall. *Geophysical Research Letters*, *48*(5), e2020GL091588. https://doi.org/10.1029/2020gl091588

Zhou, Z. Q., Xie, S. P., & Zhang, R. H. (2021). Historic Yangtze flooding of 2020 tied to extreme Indian Ocean conditions. *Proceeding Academy of Sciences of the Unite States of America*, *118*(12), e2022255118. https://doi.org/10.1073/pnas.2022255118